Materials Science Forum
ISSN: 1662-9752, Vol. 1182, pp 103-112
doi:10.4028/p-VmX8fD

Submitted: 2026-01-16
Revised: 2026-02-17
Accepted: 2026-02-17
Online: 2026-04-10

Numerical Simulation of Liquid Resin Impregnation in a Real Digitized Reinforcement during Liquid Composites Molding Processes

Mouadh BOUBAKER[1,a*], Arthur CANTAREL[1,b], Gérald DEBENEST[2,c]

[1]Institut Clément Ader, Université de Toulouse, CNRS UMR 5312, IMT Mines Albi, UPS, INSA, ISAE-SUPAERO, Toulouse, France

[2]INPT, UPS, IMFT (Institut de Mécanique des Fluides de Toulouse), Université de Toulouse, Allée Camille Soula, 31400, Toulouse, France

[a]MOUADH.BOUBAKER@iut-tarbes.fr, [b]arthur.cantarel@iut-tarbes.fr, [c]gerald.debenest@toulouse-inp.fr

Keywords: Liquid Composite Molding; Unsaturated flow; Capillary effects; Process simulation.

Abstract. Liquid Composite Molding (LCM) processes, used for producing high-quality, complex composite parts, rely on the uniform infiltration of liquid resin into fibrous fabrics. These fabrics possess a dual-scale structure: highly porous inter-tow spaces surrounding denser fiber tows. The resulting disparity in permeability and flow rates is a primary cause of defect formation, such as voids. To minimize these defects, accurate simulation, incorporating the critical influence of capillary pressure on resin infiltration within the fiber tows, is essential. This work presents a robust numerical model developed to simulate the two-phase resin flow and impregnation dynamics within a digitized, real plain-weave E-glass reinforcement obtained via X-ray micro-computed tomography (CT). The simulation utilizes the open-source multiscale multiphase solver, hybridPorousInterFoam, which employs a Darcy-Brinkman approach, transitioning between Darcy's law in porous regions and Navier-Stokes in free space. A key methodological enhancement involved modifying the advection algorithm using the isoAdvector scheme to mitigate numerical instabilities caused by the high viscosity ratio between the resin and air. Capillary effects at the mesoscale are incorporated through multiscale parameters, specifically the drag and surface tension forces. The key findings demonstrate that the modified solver successfully handles the fluid-fluid interface advection for high viscosity ratios. A parametric study highlighted the significant effect of capillary pressure on multiphase flow within the dual-scale porous media. The numerical results for flow front advancement showed very good agreement when compared against dedicated experimental validation data, confirming the model's high predictive accuracy and its potential for optimizing LCM injection conditions.

Introduction

The global demand for lightweight, high-performance composite materials necessitates highly efficient manufacturing techniques, with Liquid Composite Molding (LCM), including RTM and VARTM, being key processes [1]. A critical challenge in LCM is void formation during resin impregnation, which severely compromises structural integrity; even a 5% void content can cause a 20% reduction in interlaminar strength, leading to part rejection [2].
The primary mechanism of void creation is linked to the Capillary number (Ca), which is the ratio of viscous forces to capillary forces :

$$\mathrm{Ca} = \frac{\mu\, U}{\gamma} \tag{1}$$

where μ is the injected liquid resin viscosity, U is its velocity and γ is the surface tension between resin and air.
This force balance governs the flow distribution within the dual-scale fabric's macro- and micro-pores. Accurate modeling of capillary pressure, which significantly assists in filling the micro-scale fiber tows, is essential for optimizing saturation [3].

Conventionally, LCM flow modeling often relied on single-phase approaches, but recent work highlights the necessity of multiphase flow models to capture phenomena like capillary effects and void formation accurately [4]. However, standard interface-capturing methods (like VOF) suffer from spurious currents at the fluid-fluid interface, especially with the extremely high viscosity ratio (e.g., 10^4 to 10^5) characteristic of resin/air systems [5]. These numerical artifacts corrupt surface tension calculations, limiting the model's reliability.
Furthermore, the validation of high-fidelity models based on X-ray micro-computed tomography (CT) often lacks the rigorous multi-scale experimental confirmation needed to verify underlying dual-scale flow physics (e.g., unsaturated permeability) [6].
This study presents a novel, stabilized, two-phase numerical model for simulating resin flow in dual-scale fabrics. It utilizes the open-source, multiscale, multiphase hybridPorousInterFoam solver [7], fundamentally modified to eliminate spurious currents and enhance robustness for typical resin viscosities. The stabilized solver is used to examine the effects of capillary pressure on the multiphase flow in dual-scale porous media, simulate resin impregnation directly within realistic 3D CT-scanned geometries and perform rigorous multi-scale experimental validation against flow front advancement. This research aims to provide a reliable predictive tool for process optimization, contributing to higher saturation levels and reduced part rejection in high-performance composite manufacturing.
The remainder of this paper is structured as follows. Section 1 details the essential modification made on the multiphase multiscale hybridPorousInterFoam solver, focusing on the method used to effectively reduce spurious currents caused by high viscosity ratios. Section 2 presents a parametric study that highlights the significant impact of capillary pressure on multiphase flow within dual-scale porous media. Section 3 presents the numerical simulation of resin flow within realistic scanned geometries and its subsequent validation against experimental results, including comparisons of flow front positions and shapes. Finally, the concluding section summarizes the key findings and outlines future research directions.

Solver Modification for Spurious Currents Reduction

Accurate multiphase flow simulations, particularly those with sharp differences in fluid properties (like liquid resin and air in Liquid Composite Molding - LCM), are difficult. The main problem is spurious currents: non-physical fluid movements near the interface caused by an imbalance between the discrete calculation of capillary forces and pressure jumps. These currents are amplified with extreme property ratios (e.g., density and viscosity) and prevent simulations from reaching a stable state (equilibrium).
Volume Of Fluid (VOF) methods are widely used Eulerian approaches for directly simulating unsteady, incompressible multiphase flows. However, like all numerical methods, they have limitations particularly when capillary forces dominate. VOF methods reconstruct interfaces using a volume fraction field on a fixed grid, and the Continuum Surface Force (CSF) model is often employed to represent surface tension. However, the discrete nature of this representation, coupled with finite difference approximations of the volume fraction field, leads to significant errors in calculating interface normal and curvature. These errors, in turn, produce spurious currents that become problematic when surface tension dominates. Different methods have been attempted in the literature to minimize spurious currents and enhance surface tension modeling in different contexts [8, 9]. Comparative studies highlight that the effectiveness of different methods and reduction techniques depends on the specific flow scenario and fluid properties (such as density and viscosity ratios) and the desired level of accuracy [10].
Liquid resin used in LCM processes typically exhibits a viscosity ranging from 10^{-2} to $1\ \mathrm{Pa \cdot s}$ and a density around $1000\ \mathrm{kg/m^3}$. In contrast, the displaced air within the dry textile preform has a significantly lower viscosity, approximately $1.76 \cdot 10^{-5}\ \mathrm{Pa \cdot s}$ and a density of about $1.2\ \mathrm{kg/m^3}$. Simulating the multiphase resin flow through a dual-scale porous domain using the hybridPorousInterFoam solver, in conditions similar to those found in LCM processes, resulted in pronounced numerical instabilities at the fluid-fluid interface. These instabilities, characteristic of

spurious currents, are directly attributed to the substantial disparities in fluid properties, presenting a significant challenge to numerical stability. Initial attempts to mitigate these instabilities included mesh refinement, time step reduction, as well as modifications of the discretization schemes yielded no observable improvement which demonstrates that a fundamental modification of the solver's structure is needed, particularly in the interface tracking method used which is the VOF method. VOF schemes can be categorized into algebraic and geometric schemes. Algebraic VOF schemes (like Multidimensional Universal Limiter with Explicit Solution MULES [11]) are computationally efficient but may lack accuracy for complex interfaces and often fail to predict surface tension accurately in low capillary number flows, leading to spurious currents. Geometric schemes, in contrast, explicitly reconstruct the interface within each cell using local volume fraction data enabling more precise fluid volume flux calculations and enhancing interface sharpness and accuracy. The isoAdvector algorithm is a robust geometric VOF method designed for sharp interface advection in incompressible multiphase flows. It offers higher accuracy and better interface sharpness compared to algebraic methods like MULES, making it particularly advantageous for complex geometries and situations where surface tension effects are significant. It also excels in volume conservation and overall accuracy [12]. A key advantage of the isoAdvector algorithm is its enhanced interface sharpness. By geometrically reconstructing the fluid interface within each surface cell, it achieves a more distinct phase separation, reducing numerical diffusion at the interface. This sharper representation is crucial in simulations where surface tension and curvature effects are significant [13]. Benchmark tests and applications confirm the promising accuracy of isoAdvector in standard interface advection problems like notched disc and sphere transport in shear flow and show that it excels in volume conservation, boundedness, interface sharpness and overall accuracy compared to algebraic methods like MULES [14]. Inspired by these successful benchmark tests, we aimed to replace the MULES advection method with isoAdvector in the hybridPorousInterFoam solver to eliminate spurious currents in our simulations.

To achieve this, we developed a multi-step algorithm inspired from existing research [14], to modify hybridPorousInterFoam's advection scheme. We then conducted several tests to evaluate the modified solver's performance in maintaining a sharp and stable interface, particularly in scenarios like those encountered in Liquid Composite Molding (LCM) processes. As an example, Figure 1 showcases the solver's ability, when using isoAdvector, to effectively eliminate numerical instabilities at the fluid-fluid interface. In this test, a fluid with a viscosity of $\mu = 1\ \mathrm{Pa \cdot s}$ (shown in red in Fig. 1) is injected into a dual-scale domain (Fig. 1(a)), which is initially saturated with air (blue in Fig. 1), under a constant velocity of $1\ \mathrm{mm/s}$.

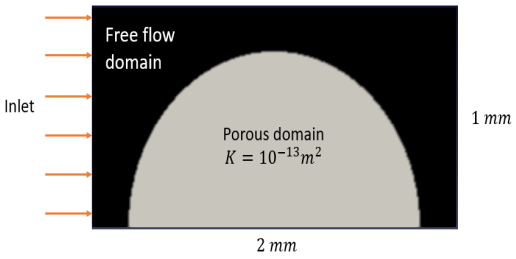

(a) Dual-scale porous domain used in this test-case

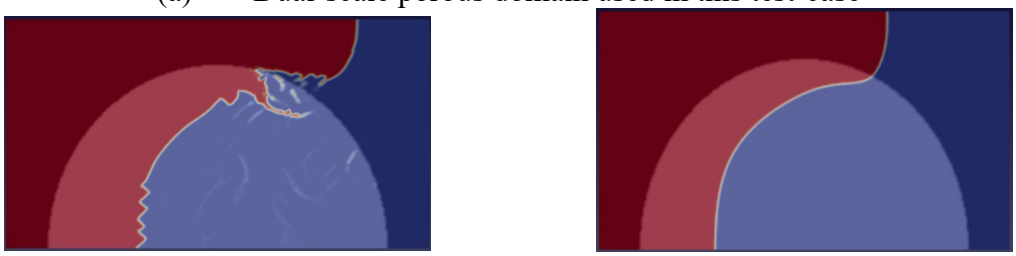

(b) MULES (c) isoAdvector

Fig. 1. MULES and isoAdvector performance in simple porous media geometry.

We successfully demonstrated the feasibility of integrating the geometric VOF algorithm isoAdvector into OpenFOAM's multiphase, multiscale solver hybridPorousInterFoam. This modification allows for the accurate simulation of test fluid injection into a dual-scale porous domain. The enhanced solver consistently produced sharper and smoother interfaces, leading to more stable simulations across various porous geometries and significantly reducing spurious currents.

Parametric Study of Capillary Effects on Mesoscale Impregnation

The hybridPorousInterFoam solver rigorously incorporates capillary effects through relative permeability, which describes the change in permeability due to the presence of a second fluid, and capillary pressure p_c, which describes the pressure difference between the two phases resulting from surface tension [7].

To assess the impact of capillary effects on resin flow simulations at the mesoscale, we will simulate the flow of a test fluid within the Representative Elementary Volume (REV) presented in Fig. 2 representing a 2x2 tow structure of a plain weave textile (Fig. 2). The porous tows have a fiber volume fraction of 0.6 and a transversal and longitudinal permeabilities estimated using Gebart model assuming a fiber radius of 12 µm. The global fiber volume fraction of the REV is 0.67. Fluid injection is driven by a pressure gradient applied between the inlet and outlet, with the REV initially saturated with air. The resin is considered as the wetting phase and the air as the non-wetting phase. This section focuses on analyzing how variations in the entry capillary pressure amplitude p_{c0} influence the resin flow dynamics, where the capillary pressure dependence on saturation is modeled using the Van Genuchten model :

$$p_c = p_{c0}(\alpha_{l,pc}^{-\frac{1}{m}} - 1)^{1-m} \quad (2)$$

with $\alpha_{l,pc}$ is the effective wetting fluid saturation and m is a non-dimensional coefficient dictated by porous media properties.

The pressure difference between the inlet and outlet was set to $\Delta P = 100$ kPa and 4 cases were investigated:

- Case 1: Neglecting the capillary effects ($p_{c0} = 0$ Pa).
- Case 2: Considering the capillary effects using Van Genuchten model for the capillary pressure (Eq. 2) with low value of $p_{c0} = 10$ Pa and $m = 0.8$.
- Case 3: Considering the capillary effects with $p_{c0} = 100$ Pa and $m = 0.8$.
- Case 4: Considering the capillary effects with higher entry capillary pressure value $p_{c0} = 1000$ Pa and $m = 0.8$.

The comparison was performed by analyzing the saturation profiles and the global domain saturation. The saturation comparison is illustrated in the cross-section shown in Fig. 2.

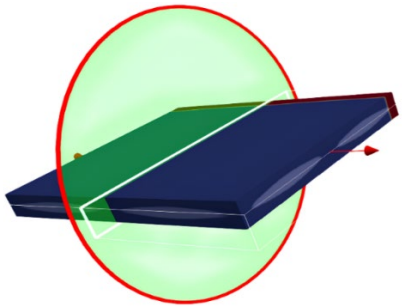

Fig. 2. Location of the cross-section used for results representation.

Due to the very low value used in Case 2, the results were similar to those obtained when capillary effects were negligible (Case 1), both saturation curves coincide and the curve for $p_{c0} = 10$ Pa was cut in Figures 4 and 5 for visualization. Conversely, Fig. 3 demonstrates the significant effect and importance of capillary forces for a higher entry capillary pressure value in impregnating the fibrous tows by comparing Case 1 and Case 3 at $t = 2.28$ s.

Case 1: Saturation of the cross-section $\alpha_l = 0{,}878$

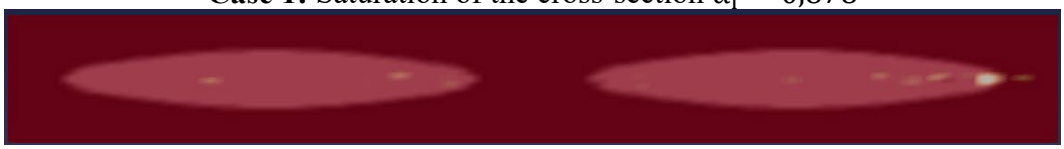

Case 3: Saturation of the cross-section $\alpha_l = 0{,}998$

Fig. 3. Comparison of liquid injection patterns between Case 1 and Case 3. (In both cases, red indicates the injected liquid, blue represents the initially present air, and clear zones denote the porous tows).

Figures 3 and 4 clearly shows a significant difference in global domain saturation between the two cases. The figures clearly show an increase in saturation when the entry capillary pressure is raised from $p_{c0} = 0$ Pa to $p_{c0} = 100$ Pa.

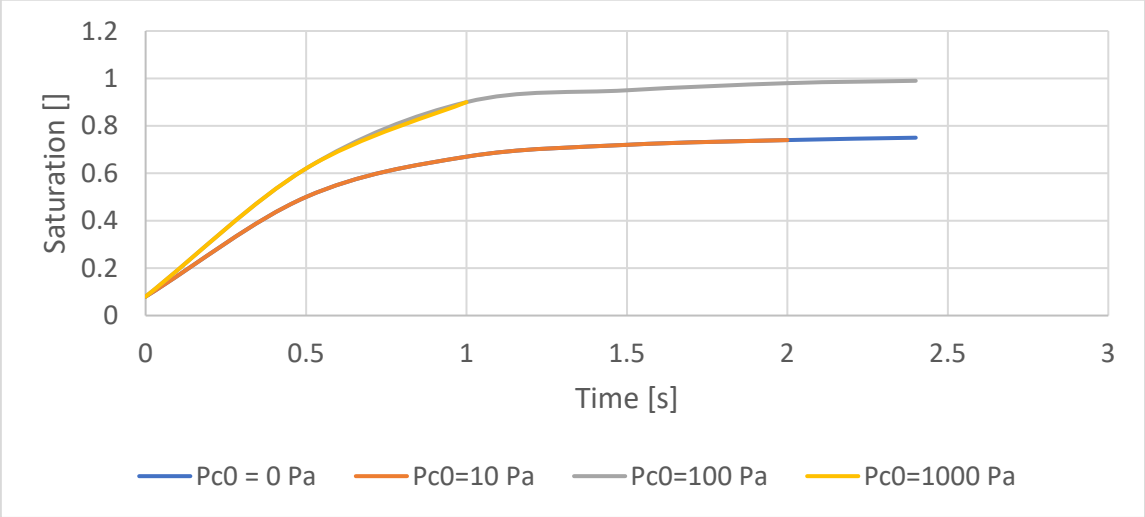

Fig. 4. Effect of p_{c0} on the domain saturation for $\Delta P = 100$ kPa.

For this pressure difference value, $\Delta P = 100$ kPa, no significant difference is observed when the value of the capillary pressure is increased to $p_{c0} = 1000$ Pa as evident in the saturation vs time plot (Fig. 4). Notably, using this higher value of entry capillary pressure drastically increases the computational time without significantly impacting the domain saturation. Consequently, the fourth test was stopped at $t \approx 1$ s.

A second case was investigated by reducing the pressure difference controlling the flow to $\Delta P = 20$ kPa, in order to examine the dependence of the entry capillary pressure's effect on the applied pressure. The same four values of p_{c0} used in the first example were tested. As observed in Figure 8, a higher capillary pressure results in increased saturation within the fibrous tows. This test demonstrates also that even with an entry capillary pressure of $p_{c0} = 1000$ Pa, the domain does not reach full saturation (achieving a maximum saturation of around 0.8). This contrasts with the first case, which used a higher applied pressure, and indicates that higher capillary pressure values are necessary to achieve full saturation when lower applied pressure values are used.

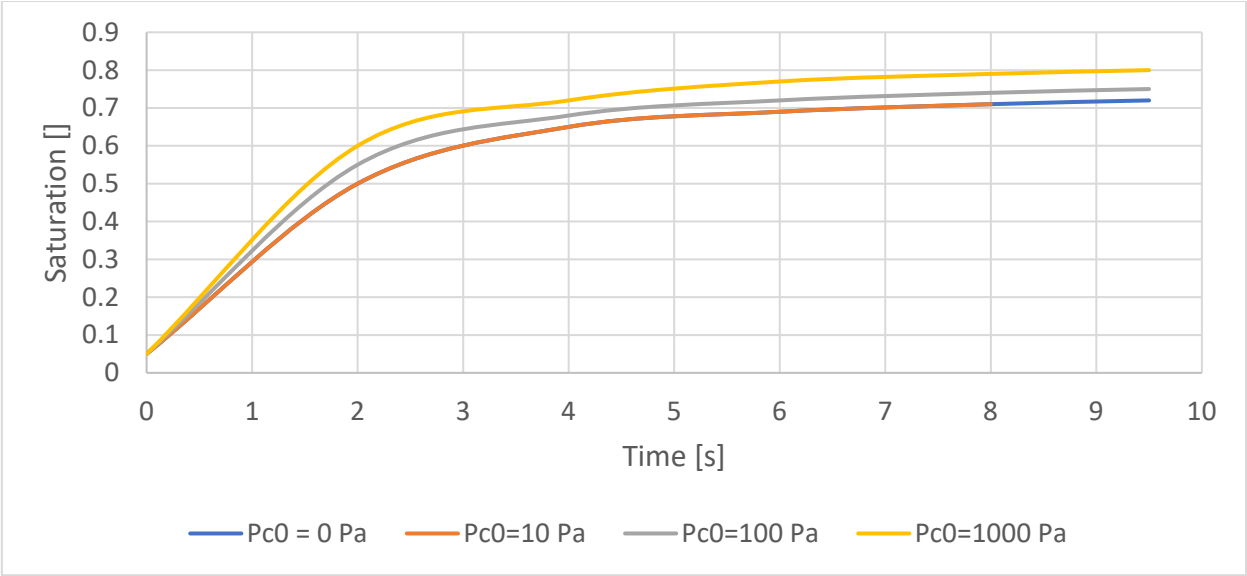

Fig. 5. Effect of p_{c0} on the domain saturation for $\Delta P = 20$ kPa.

The influence of capillary pressure on the impregnation of dual-scale porous media, and its dependence on the applied pressure magnitude, has been demonstrated. Capillary forces can be particularly significant in driving resin flow, notably during the initial impregnation stages and within densely packed fiber tows. This can be explained by the fact that at high capillary pressures, capillary effects become significant, aiding in pulling resin into the fiber tows and saturating them. However, the achievable capillary pressure is limited in this model; modeling high values of p_{c0} requires a finer mesh and necessitates longer computational time. Future research will investigate the influence of fiber volume fraction on these capillary effects and leverage the numerical model to determine the optimal injection pressure required to achieve full saturation as a function of specific flow parameters.

Simulation of Resin Flow in Realistic Scanned Geometries

To validate the capability of our numerical model in capturing the flow front positions and shapes, a dedicated experimental setup was developed. This new setup utilizes a microscope to closely monitor the flow front's advancement and shape, allowing for a precise validation and identification of the model's limitations. Experimental flow front data is crucial for the validation and optimization of simulation models. Precise monitoring provides data that can be compared against reinforcement filling simulations, helping in identifying discrepancies and allowing for the refinement of simulation models by incorporating real complexities of real reinforcements, such as varying fiber volume fraction. This leads to more accurate predictions of flow front position, fill time, and potential defect formation.

In this study, we chose to simulate liquid resin flow in a 3D scanned geometry obtained using µCT. The textile reinforcement scanned is an E-glass plain weave with a tow linear density of 2400 g/km and a nominal areal weight of 800 g/m^2. The greyscale image datasets of the multi-layer textile sample have been acquired using a laboratory-scale GE Phoenix Nanotom µCT scanner [15]. A four-layer specimen with a diameter of 40 mm was prepared to fit the in-situ compaction fixture of the scanner. The µCT data was processed in MATLAB R2023b, to accurately distinguish between inter-tow space, warp tows, and weft tows. There are two primary tasks: image segmentation and individual tow identification. Image segmentation, based on grayscale thresholding, differentiated between air and tow pixels. Three STL files, corresponding to warp tows, weft tows, and inter-tow space, were generated post-segmentation.

The experimental setup (Fig. 6) is designed for the unidirectional injection of a test fluid into a four-layer specimen placed in a circular mold. The mold consists of a 17 mm thick lower plate and a 4.8 mm thick transparent plexiglass upper plate, enabling visual tracking of the flow front. The mold itself is circular, with a 100 mm diameter and an inner circular cavity of 63 mm diameter where the

specimen is seated. The fluid is injected through a 5.5 mm circular injection port, connected via a silicone pipe to a syringe. This syringe is operated by a syringe pump, allowing for precise control of the injection flow rate. A second pipe is connected to the mold's outlet to evacuate the test fluid once the textile is saturated.

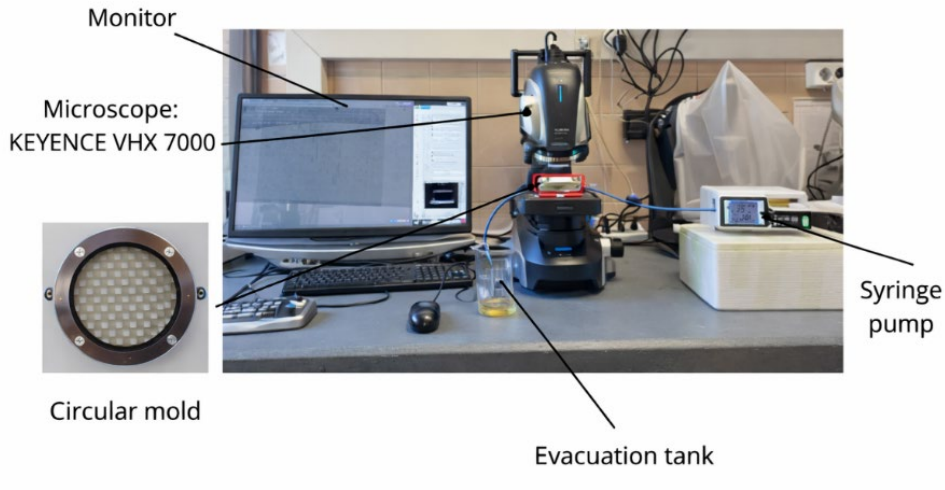

Fig. 6. Overview of the experimental setup.

Circular specimens, each consisting of four layers of the described plain weave textile, were prepared with a 63 mm diameter using a laser cutting machine. The specimen is seated in the mold's inner cavity and the mold is then closed with the upper plate and clamped using bolts to achieve the desired thickness, which corresponds to the target fiber volume fraction. The distance between the upper and lower plates h, measured using a caliper, is linked to the fiber volume fraction V_f through Eq. 3:

$$V_f = \frac{m}{\rho A h} \tag{3}$$

where m is the mass of the sample, ρ is the fiber density characteristic of the used fabric and A is the sample's planar area.

Once closed, the mold is connected to the pipes and the test fluid is injected through the inlet at a constant flow rate controlled using the syringe pump. The test fluid used is rapeseed oil, with a viscosity of $7.78 \cdot 10^{-2}$ Pa · s, a surface tension of approximately 0.032 N/m at 25° C and a density of 916 kg/m^3. The impregnation process is observed and filmed using a KEYENCE VHX 7000 microscope. An overview of the entire experimental setup is illustrated in Fig. 6.

The syringe pump enables control over the injection volumetric flow rate, ranging from 0 to 1500 ml/h. For a fiber volume fraction of 0,5, the computed sample thickness, derived using Eq. 3, is 2.68 mm (measured using a caliper). We assume the flow to be established and unidirectional once it reaches the half-way point of the mold.

A numerical simulation was conducted to model the flow in the experimental conditions, (Fig. 7). The inlet velocity was set to 1.64 mm/s, consistent with the established flow velocity imposed experimentally. Van Genuchten model (Eq. 2) was used to model the capillary effects also in these simulations for the three fiber volume fractions with $p_{c0} = 1000$ Pa and $m = 0.8$. These values were chosen to approximate the capillary pressure values found in the experimental studies of the composites applications [16].

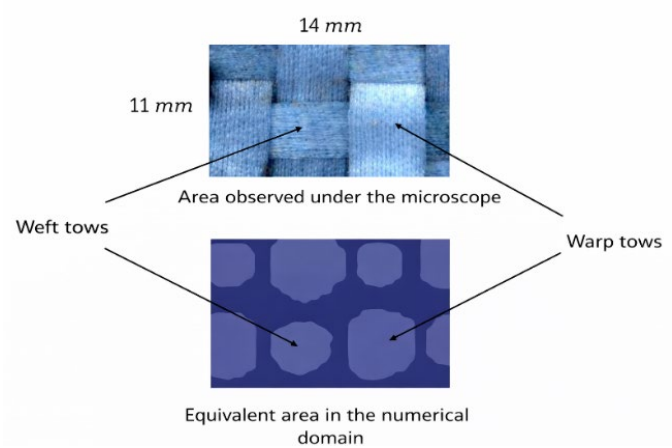

Fig. 7. Correspondence between experimental and numerical domains.

The numerical-experimental comparison encompassed both the flow front shapes and positions. Images captured using the microscope were binarized to clearly identify the flow front shapes, enabling direct comparison with simulations.

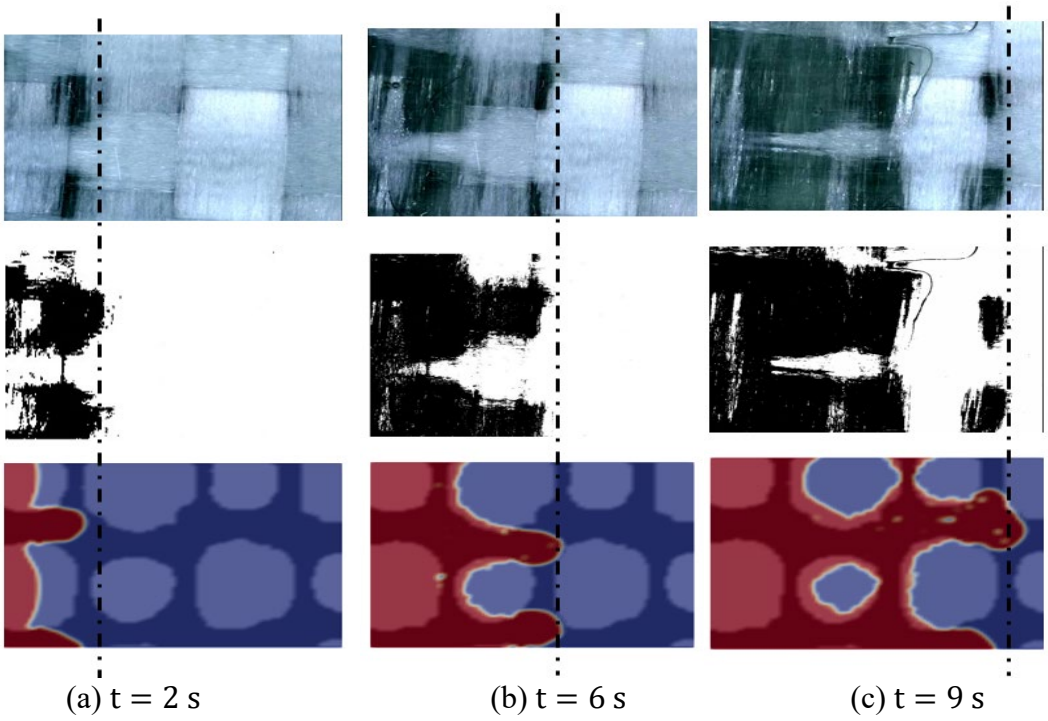

Fig. 8. Comparison between experimental and numerical flow front shapes.

From Fig. 8, we can observe that our numerical model is able to model the experimental flow front shapes. In Fig. 8 (a) and (b), the numerical simulation exhibits the same faster flow in the inter-tow spaces and slower flow inside the longitudinal weft tows and transversal warp tows. However, Fig. 8 (c) shows a limitation of the numerical geometry used in these simulations: it over-represents the inter-tow space size in the upper surface. In the numerical domain, this zone is considered a free-flow space with a larger size than the actual compacted inter-tow space on the upper surface of the real specimen, which explains the shape difference observed between the binarized and the numerical simulation images in Fig. 8 (c).

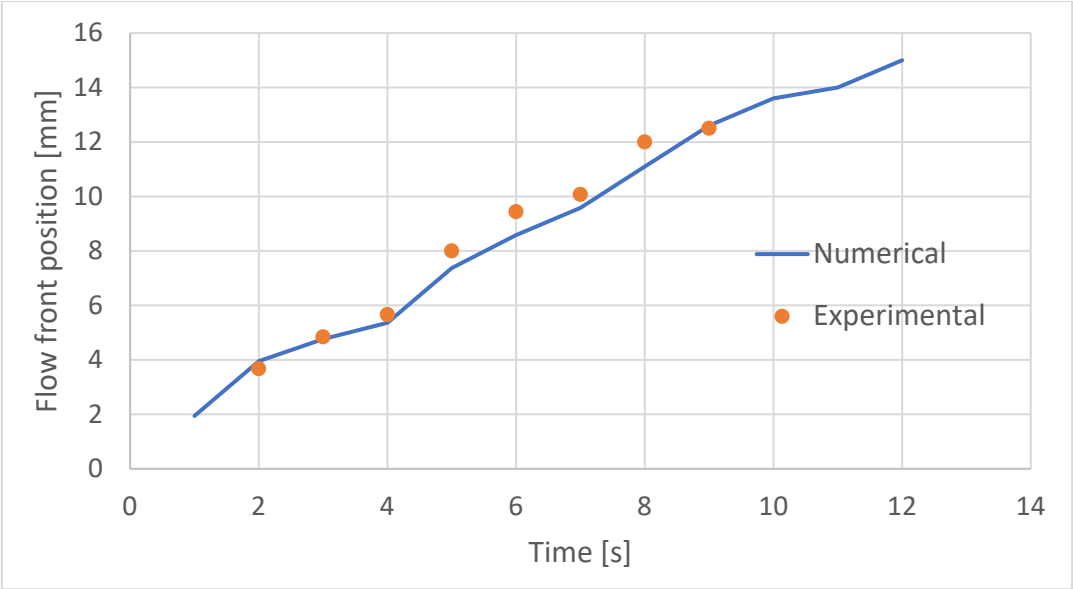

Fig. 9. Comparison between experimental and numerical flow front positions.

The numerical flow front advancement at different time steps, depicted in Fig. 9, shows overall good agreement with the experimental positions (Mean Absolute Percentage Error (MAPE) of 6%). Differences between model predictions and experimental results can stem from experimental errors or data manipulation. Experiments are susceptible to uncontrollable factors like variations in material properties and handling effects. These discrepancies can also indicate limitations in the model's underlying assumptions or the need to incorporate additional physical phenomena for greater accuracy. Numerical models inherently simplify reality by making assumptions and neglecting certain complexities (e.g. homogeneous tow permeability and porosity). Discretization errors, arising from mesh quality and time step choices, also contribute to the differences. Furthermore, manual extraction of experimental results can introduce some uncertainty.

Conclusions

This study presents the development and rigorous validation of a robust numerical multiphase, multiscale model essential for simulating resin infiltration in dual-scale composite reinforcements, specifically addressing and stabilizing the numerical instabilities caused by the extreme viscosity ratio between resin and air. This refined model demonstrated that capillary pressure significantly enhances impregnation into fiber tows, and that its impact is dependent on the applied injection pressure. By applying the solver to 3D realistic scanned geometries, the study eliminated the predictive inaccuracies of idealized configurations, achieving very good agreement against experimental data, including flow front positions and shapes. This integration of advanced computational stabilization techniques with highly accurate geometric representation provides important insight into LCM flow behavior, enabling the optimization of process parameters for the production of high-quality composite parts. Future research will focus on the influence of fiber volume fraction and extend the model to account for additional phenomena, such as tow deformability induced by resin flow and the resulting changes in local permeability. By incorporating these fluid-structure interactions, the numerical model can be leveraged to determine optimal injection parameters for achieving full domain saturation across varying textile architectures.

References

[1] Facciotto, S., Simacek, P., Advani, S.G., Pickett, A., & Middendorf, P. (2023). Modeling formation and evolution of voids in unsaturated dual scale preforms in Resin Transfer Molding processes. Composites Part A: Applied Science and Manufacturing, 173, 107675.

[2] Park, C. H., & Woo, L. (2011). Modeling void formation and unsaturated flow in liquid composite molding processes: A survey and review. Journal of Reinforced Plastics and Composites, 30(12), 957–977.

[3] LeBel, F., Ruiz, E., & Trochu, F. (2019). Void content analysis and processing issues to minimize defects in liquid composite molding. Polymer Composites, 40(1), 109-120.

[4] Gascón, L., García, J.A., LeBel, F., Ruiz, E., & Trochu, F. (2016). A two-phase flow model to simulate mold filling and saturation in Resin Transfer Molding. International Journal of Material Forming, 9(2), 229–239.

[5] Raeini, A.Q., Blunt, M.J., & Bijeljic, B. (2012). Modelling two-phase flow in porous media at the pore scale using the volume-of-fluid method. Journal of Computational Physics, 231(17), 5653-5668.

[6] Adhikari, D., Lisegaard, J.J., Pierce, R.S., Mikkelsen, L.P., Hattel, J. H., & Mohanty, S. (2025). Meso-scale permeability prediction from the multi-block 3D reconstruction of fiber reinforced polymer composite with experimental validation. Composites Science and Technology, 111290.

[7] Carrillo, F. J., Bourg, I. C., & Soulaine, C. (2020). Multiphase flow modeling in multiscale porous media: An open-source micro-continuum approach. Journal of Computational Physics: X, 8, 100073.

[8] Tong, A. Y., & Wang, Z. (2007). A numerical method for capillarity-dominant free surface flows. Journal of Computational Physics, 221(2), 506–523.

[9] Renardy, Y., & Renardy, M. (2002). PROST: A parabolic reconstruction of surface tension for the volume–of–fluid method. Journal of Computational Physics, 183(2), 400–421.

[10] Inguva, V. (2020). On methods to reduce spurious currents within VOF solver frameworks. Part 1: A review of the static bubble/droplet. Chemical Product and Process Modeling, 1. https://doi.org/10.1515/cppm-2020-0052

[11] Deshpande, S. S., Anumolu, L., & Trujillo, M. F. (2012). Evaluating the performance of the two-phase flow solver interFoam. Computational Science & Discovery, 5(1), 014016.

[12] Roenby, J., Larsen, B. E., Bredmose, H., & Jasak, H. (2017). A new volume-of-fluid method in OpenFOAM. In Marine vi: Proceedings of the vi International Conference on Computational Methods in Marine Engineering (pp. 266–277).

https://upcommons.upc.edu/handle/2117/331052

[13] Roenby, J., Bredmose, H., & Jasak, H. (2019). IsoAdvector: Geometric VOF on general meshes. In OpenFOAM® (pp. 281–296). Springer International Publishing. https://doi.org/10.1007/978-3-319-60846-4_21

[14] isoAdvector.(2025). isoAdvector/isoAdvector[C++]. GitHub. https://github.com/isoAdvector/isoAdvector (Original work published 2016) (Accessed June 24, 2025)

[15] Wijaya, W., Ali, M. A., Umer, R., Khan, K. A., Kelly, P. A., & Bickerton, S. (2019). An automatic methodology to CT-scans of 2D woven textile fabrics to structured finite element and voxel meshes. Composites Part A: Applied Science and Manufacturing, 125, 105561.

[16] Pucci, M. F., Liotier, P-J., & Drapier, S. (2015). Capillary wicking in a fibrous reinforcement - orthotropic issues to determine the capillary pressure components. Composites Part A: Applied Science and Manufacturing, 77, 133–141.